

Influence of the size-controlled TiO₂ nanotubes fabricated by low-temperature chemical synthesis on the dye-sensitized solar cell properties

Jang-Yul Kim · Tohru Sekino · Shun-Ichiro Tanaka

Received: 26 July 2010 / Accepted: 7 October 2010 / Published online: 21 October 2010
© Springer Science+Business Media, LLC 2010

Abstract Titanium dioxide nanotubes (TiO₂ NTs) with various sizes have been prepared by low-temperature chemical synthesis using commercial anatase TiO₂ particles with different crystallite size in NaOH solution and used as a photoelectrode in a dye-sensitized solar cell (DSSC). The relationship between the physicochemical properties of electrode materials and photovoltaic performance was investigated. The electrodes made from modified TiO₂ NTs showed a strong dependency on their specific surface area and resultant amount of dye adsorption; the surface area decreased with increase in the diameter of the NT from 9.8 to 23.6 nm. The conversion efficiency of the cell made from TiO₂ NT, 12.9 nm in diameter, was enhanced by 12% compared to that of the smallest NT. These results suggested that the photovoltaic performance improved by the suppression of photogenerated charge recombination in spite of a 25.3% reduction in the specific surface area. In addition, larger TiO₂ NTs could be utilized as a scattering layer on the top of the TiO₂ nanoparticulate working electrode. It was observed that this controlled TiO₂ photoelectrode architecture exhibited enhanced conversion efficiency without TiCl₄ treatment.

Introduction

Recently, titanium oxide nanotubes (TiO₂ NTs) [1–3] have been extensively studied in the field of energy creation and environmentally friendly systems. Dye-sensitized solar cell (DSSC) [4], which is a potential alternative to conventional solar cell, is considered as an application of the TiO₂ NTs. For high photovoltaic performance of DSSC, there have been significant research efforts to discover the nature of this device, which usually consists of anode electrode materials, sensitized dye, electrolyte, and counter electrode. Because anode electrode materials require nanoscale and highly crystalline semiconductors with large surface area for the adsorption of sensitized dyes, various one-dimensional (1D) nanostructured TiO₂ materials such as nanowire [5], nanorod [6–10], and nanotubes [11–29] have gained much attention.

In general, TiO₂ NTs are synthesized for the electrodes of DSSC by the electrochemical anodic oxidation method [3, 8, 11–13] or the low-temperature chemical synthesis route [2, 14], and their various tailoring structures and morphological features were investigated and determined depending on their method of synthesis. Vertically oriented TiO₂ NT arrays made by anodization of titanium in fluoride-based baths have precisely oriented nature of the NT array and excellent electron percolation pathways. However, the photovoltaic conversion efficiency [15, 16] was inferior to those of TiO₂ nanoparticle-based DSSCs owing to the insufficient surface area for dye adsorption and the relatively larger number of grain boundaries among nanoparticulate TiO₂ crystallites.

On the other hand, since Uchida et al. [17] reported DSSC of low-temperature chemically synthesized TiO₂ NTs with the cell efficiency of 2.9%, most researches have focused on the comparative study of commercial TiO₂ nanoparticles such as P25 and TiO₂ NT [18–20].

Electronic supplementary material The online version of this article (doi:10.1007/s10853-010-4994-2) contains supplementary material, which is available to authorized users.

J.-Y. Kim · T. Sekino (✉) · S.-I. Tanaka
Institute of Multidisciplinary Research for Advanced Materials,
Tohoku University, 2-1-1 Katahira, Aoba-ku, Sendai 980-8577,
Japan
e-mail: sekino@tagen.tohoku.ac.jp

Ohsaki et al. [18] reported the improved cell efficiency of 7.1% of TiO₂ NT electrode by optimizing electrode preparation condition and electrolyte composition of the cell. They analyzed electron transport properties and revealed that the TiO₂ NT electrode had a longer electron lifetime and resultant diffusion length than those of P25 electrode. Remarkably long lifetime of trapped electron in TiO₂ NT was also revealed by the photoinduced charge separation and recombination analysis using time-resolved diffuse reflectance spectroscopy, showing the advantage of 1D nanostructured TiO₂ in charge transport behavior [22]. More recently, Li et al. [20] reported the relatively high cell efficiency with TiO₂ NT of 7.6%.

Regarding to the correlation between morphology of oxide photoelectrode material and its photovoltaic performance, there are a few reports on the size effect of 1D nanostructured TiO₂ photoelectrode materials, which were prepared by electrochemical anodization route, on the DSSC performance [11, 12, 30]. For anodized TiO₂ nanotubular photoelectrodes, Ghicov et al. [12] recently reported that smaller diameters exhibited higher efficiency and pointed the importance of its aspect ratio as well as its crystallinity. These results imply that well-controlled aspect ratio of 1D nanostructured materials can provide larger photocurrent density and also result in better efficiency. In addition, it is generally argued that the architecture of the oxide photoelectrodes such as film thickness, multi-layered structure, and so on is another important factor to be considered for enhancing the DSSC performance [7, 30]. Therefore, the optimization of the balance between the diameter and thickness of 1D nanomaterial is important and required for improving the energy conversion performance.

Recently, we synthesized TiO₂ NTs with different diameters via the low-temperature solution chemical route using different sizes of raw powders [31]. However, to the best of our knowledge, the effect of the diameter of TiO₂ NT synthesized by the low-temperature chemical route on the photovoltaic properties of DSSC has rarely been reported in spite of a few reports for the anodized TiO₂ NTs electrode as mentioned before. The most significant difference between chemically prepared TiO₂ NT and anodized one is its crystallographic feature: the former one is consisted of TiO₆ octahedral network with tubular-layered compound-like structure [2, 21], while the latter one is amorphous TiO₂ or aggregate of nanocrystalline TiO₂ depending on the heat treatment [3], respectively. Therefore, the morphological characteristic of chemically prepared NT might strongly influence on the charge transport and/or recombination properties as the oxide photoelectrode.

In this study, we fabricated the photoelectrode using a series of different-sized TiO₂ NTs synthesized by low-temperature chemical route, which have an open-end nanotubular structure, and investigated the relationships

between morphological characteristics of TiO₂ NTs and their photovoltaic performance as anode electrodes at two aspects. The first one is systematical study of the influence of various sized 1D nanostructured TiO₂ NTs photoelectrode on the DSSC performance using the conventional single-layered electrode structure. Secondly, to investigate the major contribution of electron transport or light scattering in photovoltaic performance, we architecturally designed double-layered electrode by adapting modified TiO₂ NTs as a scattering layer on the TiO₂ nanoparticulate layer (here we used commercial P25 powder). Based on the results, we discuss in detail regarding the critical factor of photoelectrode in photovoltaic performance.

Experimental

Preparation of size-controlled TiO₂ NTs

The TiO₂ NTs with different crystallite sizes were prepared by annealing commercial anatase powders (Kojundo Chemical Lab. Co., Ltd., Tokyo, Japan) in a furnace at 500, 1000, and 1300 °C for 4 h [31]; hereafter, preannealed TiO₂ powders are denoted as A, and heat-treated ones are, A 500, A 1000, and A 1300, respectively, for the above-mentioned temperatures. The TiO₂ powder (1 g) and 100 mL of a 10-M NaOH aqueous solution were placed in a 250-mL Nalgene bottle and then treated in an oil bath for 62 h at 110 °C after 30 min of ultrasonication, as described in some other studies [2, 14]. To eliminate the residual Na ion in the TiO₂ NTs and to prevent its influence, we performed the ion-exchange process using 0.1 M HCl and distilled water. The precipitate was filtered and dried at 70 °C for 24 h to obtain nanotubular powders (similar to A, this is also denoted as TNT, TNT 500, TNT 1000, and TNT 1300, respectively). The fundamental morphological properties are summarized in Table 1.

Fabrication of DSSC

In the present study, synthesized TiO₂ NTs and commercial TiO₂ P25 (Degussa, Germany) powders are used for the

Table 1 Morphological properties of synthesized TiO₂ NTs: crystallite size of its raw materials [31], typical diameter of synthesized TiO₂ NTs, and specific surface area

Sample name	Crystallite size of raw materials (nm)	Diameter of TiO ₂ NTs (nm)	Specific surface area (m ² /g)
TNT	54.3	9.8	282
TNT 500	62.6	12.9	225
TNT 1000	74.0	19.1	115
TNT 1300	117	23.6	105

preparation of pastes. The pastes containing powders with ethyl cellulose and α -terpineol in ethanol were dispersed through ball milling for 24 h at 300 rpm. The films (10 μm) were deposited on the conducting F-doped tin oxide (FTO) coated glass (Pilkington TEC 8, sheet resistance 8 Ω/\square) via the screen printing method. For the desired thickness of about 10 μm , the screen printing procedure was repeated four or five times and then dried for 10 min at 125 $^{\circ}\text{C}$ to evaporate volatile components of the paste. The electrodes coated with the pastes were gradually heated under an air flow at 500 $^{\circ}\text{C}$ for 30 min to remove the organic loads and to improve the interconnection of the particles. The corresponding cells are denoted by their powder names.

To investigate the role of modified TiO_2 NTs as a scattering layer, the double-layered working electrode architecture was also fabricated as follows. The first layer was prepared on the FTO substrate using P25 paste prepared in a way similar to the method mentioned above. Then the modified TiO_2 NTs pastes were deposited on the P25 film, maintaining the thickness of about 4 μm . The next procedure is the same as the above method. In addition, commercial paste Ti-Nanoxide R/SP (named as R hereinafter, Solaronix Inc., Switzerland), which consisted of 400-nm anatase particles, was used as a reference for the scattering layer on a pre-existing nanostructured P25 TiO_2 electrode. Thus, 14- μm -thick double-layered electrodes were fabricated and named TNT/P25, TNT 500/P25, TNT 1000/P25, TNT 1300/P25, and R/P25.

The TiCl_4 treatments were performed, if required, by soaking the electrodes in 40 mM TiCl_4 aqueous solution at 70 $^{\circ}\text{C}$ for 30 min followed by water and ethanol rinse solutions and then heating at 450 $^{\circ}\text{C}$ for 30 min. After the electrodes naturally cooled to 80 $^{\circ}\text{C}$, it was immersed into a 0.3-mM ethanolic solution of N719 (commercially available ruthenium-based dye $[\text{RuL}_2(\text{NCS})_2]:2$ TBA, from Solaronix Inc., Switzerland) at room temperature for 24 h. They were then rinsed sufficiently with anhydrous ethanol to remove excess dye from the surface and air dried at room ambient.

Counter electrodes were prepared by thermal decomposition of hexachloroplatinic(IV) acid hexahydrate that was dissolved in anhydrous isopropanol. A drop of 5-mM solution was put and spread on the clean FTO substrate and dried in air. Coated electrodes were annealed at 400 $^{\circ}\text{C}$ for 30 min. The dye-sensitized electrode and the counter electrode were carefully separated by a 50- μm Surlyn sheet (Dyesol Ltd., Australia) and sealed by heating. The active area of cells was 0.25 cm^2 . The electrolyte solution, which composed 0.1 M LiI , 0.05 M I_2 , 0.6 M 1,2-dimethyl-3-propylimidazolium iodide (DMPII), and 0.05 M *tert*-butylpyridine in acetonitrile, was introduced into the interspaces between cells by capillary action.

Characterization

The overall phase of raw materials and synthesized NTs were analyzed using an X-ray diffractometer (XRD, RINT 2200, Rigaku Co., Tokyo, Japan) with $\text{Cu K}\alpha$ radiation ($\lambda = 0.15418$ nm). The surface morphology and microstructures of samples were investigated by field emission scanning electron microscopy (FE-SEM, S-4100L, Hitachi, Ltd., Tokyo, Japan) and high-resolution transmission electron microscopy (HR-TEM, JEM-2010, JEOL Ltd., Tokyo, Japan, 200 kV). Specific surface areas of the samples were estimated using nitrogen adsorption-desorption isotherm by the Brunauer–Emmet–Teller (BET, NOVA 1000, Quantachrome, Florida, USA) method. The samples were degassed for 1 h at 105 $^{\circ}\text{C}$ under vacuum. Optical spectra at ultraviolet (UV) and visible (vis) regions of the electrode films were recorded (V-670 UV–VIS–NIR Spectrophotometer, JASCO, Japan) to investigate the optical properties.

Sheet resistivity measurements for the prepared photoelectrodes were performed by the van der Pauw method (Resitest 8300, Toyo Corporation, Tokyo, Japan) at temperatures from room to 600 $^{\circ}\text{C}$ to evaluate the electrical properties of the electrodes and to determine the annealing temperature of the oxide photoelectrode layer; oxide layers were screen-printed onto the pure glass substrate to eliminate the conduction in the FTO surface layer and then used to measure the resistivity up to the temperature. The photocurrent–voltage characteristics of the cells were measured using a digital source meter (Keithley model 2400, Tokyo, Japan) by applying external potential bias to the cell under illumination through light with an energy of 100 mW/cm^2 (OTENTO-SUNIII, Bunkoh-Keiki, Tokyo, Japan). The light intensity of the illumination source was calibrated using a standard silicon photodiode (BS520, Bunkoh-Keiki, Tokyo, Japan).

Results and discussion

Morphological characteristics of materials for anode electrode

The electrode materials for DSSCs were synthesized by low-temperature chemical synthesis using commercial anatase TiO_2 nanoparticles, which were obtained at various annealing temperatures. Figure 1 shows their enlarged XRD peaks at (101) and (110). As the annealing temperature increased, grain growth occurred in the powder. XRD analysis revealed that when the annealing temperature was below 650 $^{\circ}\text{C}$, the samples contained the anatase phase. Both anatase and rutile phases appeared in the present sample annealed at 1000 $^{\circ}\text{C}$ implying that phase

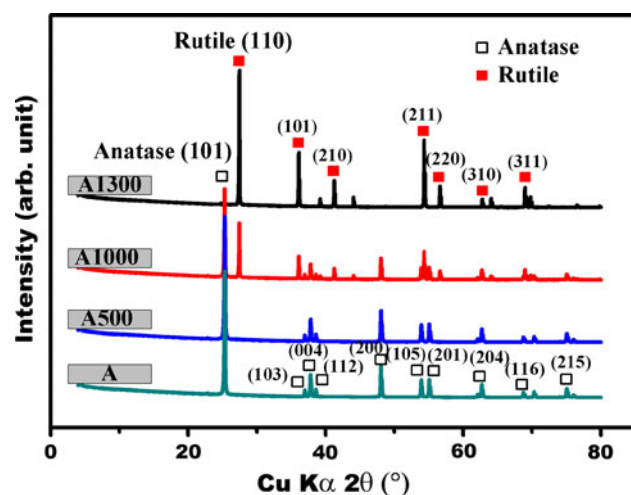


Fig. 1 X-ray diffraction patterns of TiO_2 powder as a starting material prepared at various annealing temperatures

transformations occurred in the temperature range 600–1100 °C, depending on the preparation conditions, particle size, and the presence of impurities [32–34]. On the other hand, the anatase phase disappeared at an annealing temperature of 1300 °C, indicating that the complete anatase to rutile phase transformation occurred between these temperatures (1000–1300 °C). The average crystallite size was estimated from the line broadening of the X-ray diffraction reflections of the (101) and (110) peaks of anatase and rutile TiO_2 , respectively, using the Sherrer formula [35]. As can be seen from Fig. 1 and Table 1, increasing the annealing temperature increased the crystallinity of TiO_2 powder and, accordingly, the growth of TiO_2 crystallites.

Figure 2 shows TEM images of as-synthesized TiO_2 NTs, indicating crystallite size dependency of the starting materials on the product morphology. The diameter of individual NTs is 9.8 nm (a), 12.9 nm (b), 19.1 nm (c), and 23.6 nm (d), respectively. Even though TNT 1300 shows the form of overlapped NTs owing to the aggregation tendency of TiO_2 NTs (see ESM, Fig. 1S), the diameter of a single NT is more than two times the diameter of TNT. Therefore, the typical diameter of synthesized TiO_2 NTs is proportional to the TiO_2 particle size used for chemical synthesis.

Figure 3 shows the adsorption–desorption isotherms of as-prepared TiO_2 NTs samples for synthesis duration of 62 h. The isotherms indicate a typical IUPAC type IV patterns, suggesting that pore volume decreases as the crystallite size of raw materials increase. The hysteresis loops of TNT and TNT 1000 are similar to those of TNT 500 and TNT 1300, respectively. From the BET curves, it could be inferred that the larger diameter of TiO_2 NTs might not be suitable for photoelectrode materials, because specific surface area is directly related to the amount of dye

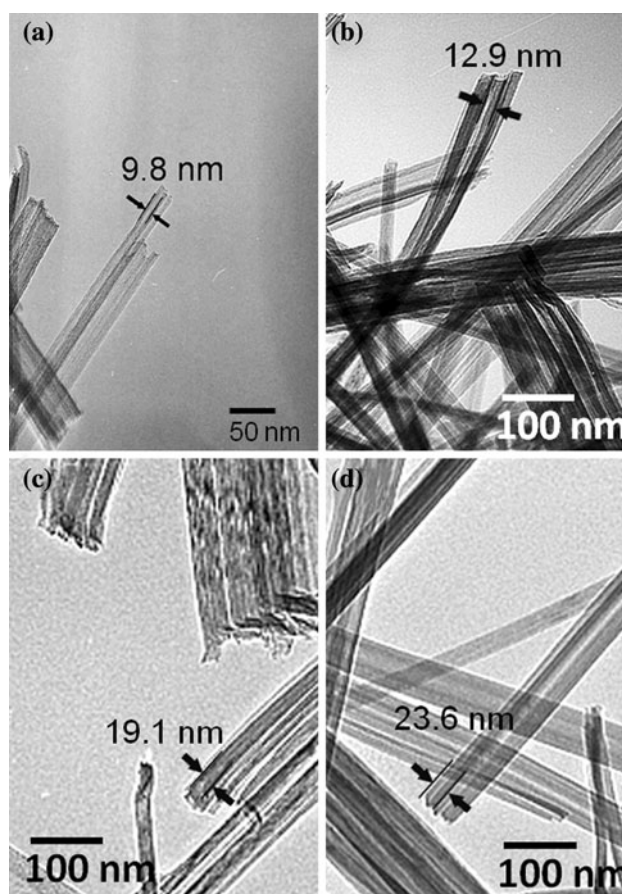


Fig. 2 TEM images of synthesized TiO_2 NTs after soft chemical method with **a** A; **b** A 500; **c** A 1000; **d** A 1300, showing their typical diameters

adsorption, and it would result in the decrease of short current density (J_{sc}) and conversion efficiency of cell.

Table 1 summarizes morphological property comparisons of modified TiO_2 NTs. Crystallite sizes of raw materials that were estimated through XRD measurement [31] are closely related to the typical diameter of individual TiO_2 NTs (measured from TEM images) and specific surface area of synthesized TiO_2 NTs. Consequently, it is reasonably considered that the morphological characteristics can be controlled by the synthesis condition of the present oxide NT.

Electrical properties of oxide photoelectrodes

Figure 4 shows the temperature dependency of sheet resistivity of anode photoelectrodes (i.e., P25 and representative modified TiO_2 NT, TNT 500) with a thickness of 10 μm , which was prepared on the insulating glass substrate to eliminate the effect of FTO coating. The resistivity was measured at temperatures from room to 600 °C during the heating and cooling process. It is essentially important

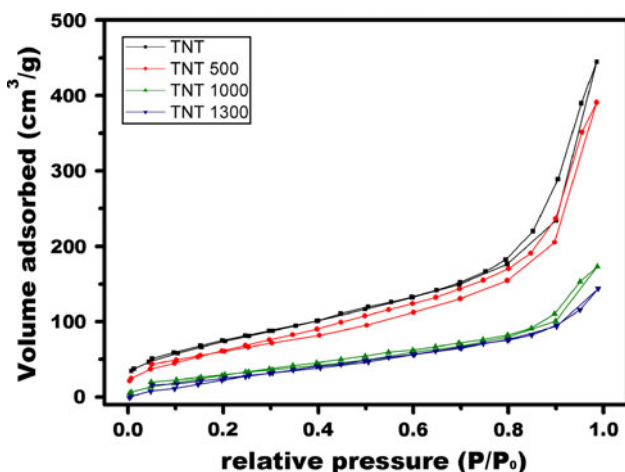


Fig. 3 Nitrogen adsorption–desorption isotherms of as-prepared TiO₂ NTs obtained by low-temperature chemical synthesis of 62 h reaction duration

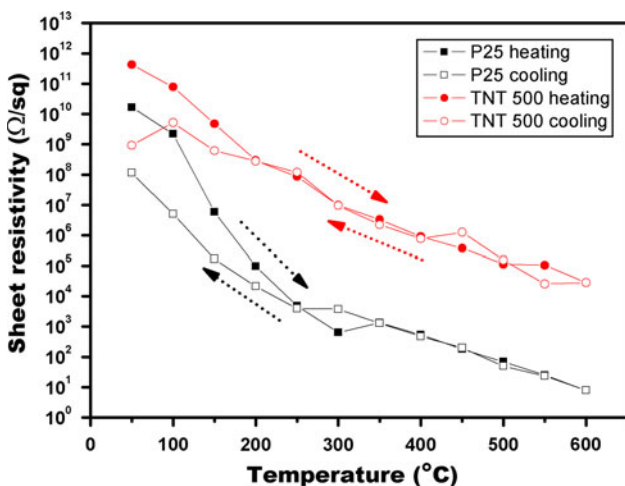


Fig. 4 Resistivity comparison of P25 and TNT 500 as a function of temperature (thickness of 10 μm)

to control the resistivity of the bulk electrode, which is an important parameter that decreases cell efficiency. In particular, as the shape of the material or morphological properties possibly affect the results, it is worthwhile to investigate the sheet resistivity of the electrode consisting of nanocrystalline oxide materials with high intrinsic resistivity. Four-point-measurement techniques, such as the van der Pauw method [36], are suitable to investigate the effect caused by the bulk as well as the overall resistivity of the electrode samples.

It was revealed that sheet resistivity of both P25 and TNT 500 electrodes decreased with an increase in the test temperatures; this behavior was also confirmed for the other modified TiO₂ NTs (not shown in Fig. 4). This variation is considered because of the intrinsic nature of the semiconductor material as well as the elimination of

organic components that were used to prepare the coating paste and that followed improvement of the mechanical contact of particles (thus sintering of oxides). The sheet resistivity values of P25 were mostly lower than those of TNT 500 regardless of heating, and for both cases, the resistivity after heating was lower because of the consolidation of the oxide layers. However, after returning to room temperature, the sheet resistivity of the TNT 500 electrode exhibited more than two orders of lower value than before, while that of P25 was around two orders of decrease in magnitude.

These characteristics of sheet resistivity for P25 and modified TiO₂ NT may result from the essential difference between three-dimensional (3D) spherical nanoparticles and 1D NTs; nanoparticulate material generally has better sinterability owing to the equiaxial shape, smaller size, and resultant high driving force of coalescence. In other words, higher heating temperature results in a dense nanoparticulate oxide layer. In the case of 1D nanomaterials, however, sinterability is considered to be lower than the nanoparticulate system, implying that the NTs can maintain higher porosity and surface area. All these structural features affect the total conversion efficiency in photovoltaic electrode applications. In the present TiO₂ systems, although the sheet resistivity of electrodes decreased depending on the heating temperature, it should, however, be noted that the surface area also significantly decreased after sintered at 500 °C, which would result in the decreased amount of the adsorbed dye. Therefore, it is important to optimize the annealing temperature at which better crystallinity and high surface area achieved, while excess neck growth between the NTs should be prevented. The annealing temperature was then fixed to be 500 °C, which was determined after SEM and BET analyses for the samples annealed at different temperatures by considering the above-mentioned morphological features and the specific surface area of samples.

J–V curves of modified TiO₂ NT DSSC

Figure 5 shows the photocurrent density–voltage (*J–V*) curves of single-layered electrodes with modified TiO₂ NTs after the TiCl₄ treatment. The *J–V* curves under the dark condition are also plotted. Their DSSC performances which were obtained from each *J–V* curve as well as characteristic values are summarized in Table 2.

The overall cell efficiency (η) and fill factor (FF) for the DSSCs coated with various samples are calculated as the following equation.

$$\eta (\%) = \left[\frac{V_{oc} \times J_{sc} \times FF}{P_{input}} \right] \times 100, \tag{1}$$

where the V_{oc} is the open circuit voltage, J_{sc} is the short circuit current density, P_{input} is the intensity of the incident

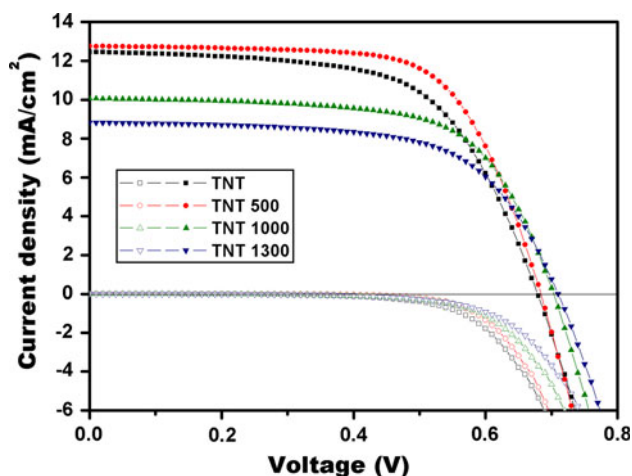


Fig. 5 Photocurrent density–voltage (J – V) curves of modified TiO_2 NTs using N719-sensitized photoanodes after TiCl_4 treatment measured under 100 mW/cm^2 simulated AM 1.5G sunlight. The J – V curves in the dark are also plotted with open symbols

light (In this experiment, the P_{input} is fixed at 100 mW/cm^2), and FF is defined as the equation

$$\text{FF} (\%) = \left[\frac{V_{\text{max}} \times J_{\text{max}}}{V_{\text{oc}} \times J_{\text{sc}}} \right] \times 100, \quad (2)$$

where the $V_{\text{max}} \times J_{\text{max}}$ is the maximum power point, P_{max} the product of J – V at the maximum power point. Among the investigated samples, TNT 500 exhibited the highest cell performance, presenting a J_{sc} , V_{oc} , FF, and cell efficiency of 12.8 mA/cm^2 , 0.683 V , 0.668 and 5.83% , respectively. It is reasonably understood that TNT 500 shows the highest cell efficiency because it has sufficient surface area and amount of adsorbed dye. Furthermore, it is likely that conversion efficiency is directly proportional to the amount of adsorbed dye, specific surface area, and J_{sc} . However, considering the fact that TNT 500 demonstrated smaller specific surface area and amount of adsorbed dye than those of TNT, there might be another factor that more dominantly affects the cell performance, specifically on the electron transport properties.

Although it is not a direct method to detect the recombination process, the comparison of the dark currents of

samples could provide information about the formation of the energy barrier on the surface of the electrode [37, 38]. However, in the present DSSCs, at high forward bias ($>0.4 \text{ V}$), dark current values decreased with an increase in the diameter of the modified TiO_2 NTs; at the same bias voltage, the dark current value decreased with an I_3^- ions on the electrode surface for the larger diameter of TiO_2 NTs. In other words, the larger size of TiO_2 NT results in the degradation of the surface area for adsorption of iodide and, consequently, promotes a decrease in the number of the surface recombination sites and resultant V_{oc} increase [39].

In addition, the decrease in the dark current with greater diameter is attributed to a rise in V_{oc} . This is in accordance with Eq. 3, which shows that V_{oc} is mainly related to the electron density in the conduction band [40] and the number of surface recombination sites:

$$V_{\text{oc}} = \left(\frac{kT}{e} \right) \ln \left(\frac{J_{\text{inj}}}{n_{\text{cb}} k_{\text{et}} [\text{I}_3^-]} \right), \quad (3)$$

where k and T are the Boltzmann constant and the cell temperature, respectively. e is the charge on the electron, J_{inj} is the injected electron current, n_{cb} is the concentration of electrons at the TiO_2 surface, and k_{et} is the rate constant for the reduction of I_3^- by conduction band electrons. From the above equation, it can be assumed that V_{oc} is inversely proportional to the recombination rate, and the greater diameter of TiO_2 NT results in an increase of V_{oc} . The injection rate of electrons to the larger diameter of TiO_2 NT surfaces was also reduced owing to the decreased amount of the adsorbed dye. Therefore, despite of drop in J_{sc} , V_{oc} increased, and there was compensation for concentration of electrons at the TiO_2 surface or reduction in I_3^- by electrons in the conduction band of the oxide NT photoelectrodes.

J – V curves of double-layered DSSC

In general, double-layered electrode architecture, which consists of transparent layer (TiO_2 particle size is about 20 nm) and light scattering layer (400 nm), is considered to

Table 2 Photocurrent density–voltage curves of modified TiO_2 NTs using N719-sensitized photoanodes after TiCl_4 treatment

Sample name	J_{sc} (mA/cm^2)	V_{oc} (V)	V_{dc} (V)	FF	Cell efficiency (%)	BET surface area (m^2/g)	Amount of adsorbed dye (mol/cm^2)
TNT	12.5	0.679	0.608	0.61	5.19	282	1.46×10^{-7}
TNT 500	12.8	0.683	0.622	0.66	5.83	225	1.11×10^{-7}
TNT 1000	10.1	0.703	0.637	0.65	4.63	115	8.62×10^{-8}
TNT 1300	8.82	0.710	0.655	0.63	3.97	105	7.23×10^{-8}

The J – V curves in dark are also plotted with open symbol lines. V_{dc} value was measured at the dark current density of -2 mA/cm^2 . BET data are obtained from as-synthesized TiO_2 NTs without annealing

improve the cell performance by increasing the amount of adsorbed dye on the surface of electrode and the light scattering effect in the electrode [41]. Figure 6 shows the J - V curves of double-layered electrodes fabricated with modified TiO_2 NTs on the P25 electrode (a) before and (b) after TiCl_4 treatment. In the case of modified TiO_2 NT with a single-layered electrode, the contribution of a larger diameter of TiO_2 NT on the photovoltaic performance is not very significant; however, it is worthwhile to investigate the photovoltaic characteristics of modified TiO_2 NTs as a light scattering layer.

Because the diameter of TNT 1300 was more than two times larger than that of TNT and its specific surface area was reduced as discussed in BET results (see Table 1 and Fig. 3), dye absorbable sites would certainly be decreased. However, when the modified TiO_2 NTs are deposited as a double-layered structure on the P25 nanoparticle electrode, it is expected that the cell efficiency will be affected by the excited electron transport or trapping of incident light.

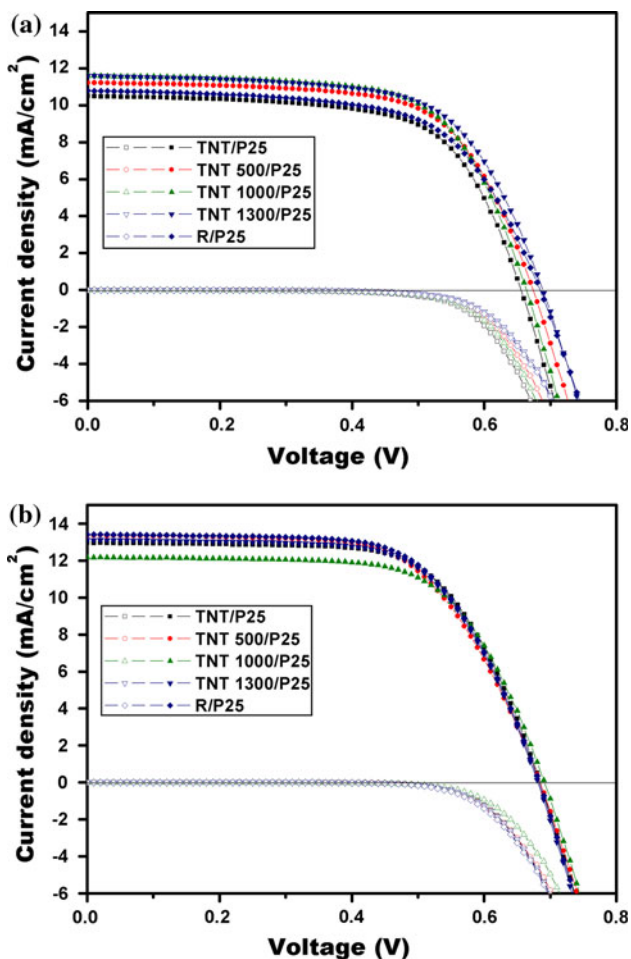


Fig. 6 Photocurrent density–voltage curves (J - V) of double-layered structures of modified TiO_2 NTs/P25 using N719-sensitized photoanodes **a** before TiCl_4 treatment and **b** after TiCl_4 treatment. The J - V curves in dark are also plotted with *open symbol lines*

The J_{sc} , V_{oc} , FF, and conversion cell efficiency of the double-layered DSSC are summarized in Table 3. Photovoltaic results before TiCl_4 treatment shown in Fig. 6a exhibited that TNT 1300/P25 had the best performance among the modified TiO_2 NT photoelectrodes, and the cell efficiency exhibited the proportional dependency on the diameter of TiO_2 NT. When the P25 underlayer was incorporated to the TNT 1300 layer (TNT 1300/P25), the J_{sc} increased from 8.82 to 11.6 mA/cm^2 , and the conversion cell efficiency was enhanced from 3.97 to 5.12% in comparison to those of single-layered geometry (TNT 1300, see Table 2) that corresponded to each increment of 31.3 and 29.0%, respectively. This is mainly ascribed to the light scattering effect in adequately enlarged TiO_2 NTs incorporated in the electrode, which may lead to enhancement of the photoresponse to infrared light [42]. In single-layered modified TiO_2 NT, the cell efficiency was decreased along with increasing diameter (Table 2) because of the reduction of adsorbed dye. Regardless of similar materials, however, the TiO_2 NTs play a significant role in improving the cell efficiency (Table 3) when they are combined with the 10- μm -thick P25 underlayer electrode, probably owing to the trapping of the incident light. With respect to the morphological characteristics of modified TiO_2 NTs, it is possible to infer that electron transport might not be improved because it is not well-connected to the interface between P25 and TiO_2 NT owing to packing difficulty. In addition, the closed-packing, which could be explained in terms of packing density of the photoelectrodes, is more difficult for NTs than that for nanoparticles. This was indirectly verified by the sheet resistivity of the electrode, showing the intrinsic structural difference between 3D spherical nanoparticles and 1D NTs as previously discussed.

The main role of large particles incorporation onto the transparent oxide electrode is certainly to enhance the photoresponse of cell to infrared (IR) light, because Ru dyes (N719) have low light absorption capability in the IR region [42]. The widely used scattering layer material is anatase TiO_2 consisting of 400-nm-sized particles on top of the active layer as stated previously. The scattering layer material should be well considered in the fact of both improvement of light harvesting efficiency and counteract such as reduction of surface area and light loss due to back-scattering. The change in the refractive index between the active layer and the scattering layer as well as the chemical bonding strength between particles and N719 are also critical factors.

As mentioned before, physical and optical properties as well as architectures of photoelectrode oxides play critical roles in improving the cell efficiency by contributing to electron transport path and light scattering effect. The double-layered structure of TiO_2 NTs on TiO_2

Table 3 Photocurrent density–voltage curves of double-layered structures of modified TiO₂ NTs/P25 using N719-sensitized photoanodes (a) before TiCl₄ treatment and (b) after TiCl₄ treatment

Sample name	J_{sc} (mA/cm ²)	V_{oc} (V)	FF	Cell efficiency (%)	Amount of adsorbed dye (mol/cm ²)
(a)					
TNT/P25	10.49	0.655	0.65	4.47	1.86×10^{-7}
TNT 500/P25	11.21	0.673	0.65	4.92	2.19×10^{-7}
TNT 1000/P25	11.60	0.663	0.65	5.04	2.02×10^{-7}
TNT 1300/P25	11.58	0.688	0.64	5.12	1.63×10^{-7}
R/P25	10.97	0.703	0.67	5.21	1.18×10^{-7}
(b)					
TNT/P25	12.97	0.684	0.65	5.83	2.02×10^{-7}
TNT 500/P25	13.36	0.684	0.62	5.75	1.75×10^{-7}
TNT 1000/P25	12.18	0.691	0.65	5.55	1.86×10^{-7}
TNT 1300/P25	13.11	0.681	0.64	5.79	1.88×10^{-7}
R/P25	13.42	0.683	0.64	5.88	1.46×10^{-7}

nanoparticles (P25) in the present study definitely showed the diameter effect of TiO₂ NTs. From UV–Vis reflectance spectra analysis for the TiO₂ NTs with various sizes and nanoparticles (P25), it is found that the reflectance of TiO₂ NTs becomes higher as the diameter of NT increases (see ESM, Fig. 2S). It is rationalized that higher reflectance contributes to the enhanced light scattering and resultant increase in light absorption by dye molecules, which phenomena finally enhance the photovoltaic efficiency. However, with respect to the structural feature, 3D material 400-nm-sized anatase “R” seems superior to 1D TiO₂ NTs, since the photovoltaic properties of R/P25 showed slightly higher performance than that of 1D TiO₂ NTs (Table 3). More specifically, J_{sc} and amount of adsorbed dye are lower than those of the other TiO₂ NTs electrodes (Table 3a). These factors mean that the scattering effect is dominant in R/P25 system. This might be ascribed by the size and morphology of primary particle. Even though TiO₂ NTs existed as aggregates with high aspect ratio in the electrode film, the largest diameter of TiO₂ NT, TNT 1300, is only 23.6 nm in TEM observation, which is comparatively smaller than 400 nm TiO₂ particle (R) as well as smaller than the wavelength of visible light. Nevertheless, the fact that TNT/P25 system has almost similar efficiency to R/P25 cell implies that TiO₂ NTs used as scattering layer have sufficient amount of adsorbed dye on the surface owing to their high specific surface area.

Furthermore, by comparing the overall V_{oc} of single- and double-layered electrodes, it was observed that the double-layered structure decreased owing to an increase in the electrode thickness. The behavior of V_{oc} in the double-layered structure also showed the opposite tendency to the single-layered electrode; both V_{oc} and conversion cell efficiency tended to increase with the larger diameter of TiO₂ NT, which was dissimilar to the single-layered electrode.

On the other hand, it was revealed that the conversion cell efficiency became consistent in the range from 5.55 to 5.83% after TiCl₄ treatment. This is regarded as the contribution of the TiCl₄ treatment, which is thought to deposit a layer of TiO₂ 1–2-nm thick on the surface of the porous film [43]. In other words, when the diameter of the modified TiO₂ NT in the second layer on the P25 underlayer was larger, the role of TiO₂ NT electrode as a scattering layer could be more effective than that of the connection of particle grains; whereas, when the diameter was smaller, the role of TiO₂ NTs as a scattering layer was less effective. However, the electron transport was improved by TiCl₄ treatment because of the improvement in connections between the particle grains present in a thick nanoporous layer. Thus, charge recombination may be more suppressed, when the diameter of TiO₂ NTs can be selected appropriately for the improvement of the electron pathway and the reduction of light loss.

Conclusion

The modified TiO₂ NTs, which have successfully been synthesized using TiO₂ anatase powder with different crystallite sizes, were utilized as photoanodes for DSSC. When TNT 500 having 12.9 nm diameter was used as a single-layered electrode, the DSSC demonstrated the highest cell efficiency and photocurrent density. This is ascribed to the enhancement of electron transport with increased TiO₂ NT diameter without serious degradation of specific surface area.

On the other hand, the largest diameter of TiO₂ NT (TNT 1300, $d = 23.6$ nm) exhibited lower photovoltaic performance because accelerating the electron transport was not sufficient owing to the reduced specific surface area. These results indicate that it is important to

understand not only the influence of 1D morphological property on the photovoltaic performance but also the well-defined size-shaped aspect ratio of electrode materials. However, it was found that larger diameter, such as TNT 1300, was suitable for the double-layered electrode architecture without TiCl_4 treatment. This observed improvement in the photovoltaic performance is attributed to the contribution of light scattering effects, which improves the light absorption rather than the electron transport.

Acknowledgements This work was supported by the Global COE (Center of Excellence) Program, “Materials Integration (International Center of Education and Research), Tohoku University,” MEXT (Ministry of Education, Culture, Sports, Science and Technology), Japan, and partly supported by the Japan Society for the Promotion of Science (JSPS) under the Grant-in-Aid for Scientific Research (A). The authors gratefully acknowledge Prof. T. Sato and Prof. S. Yin (IMRAM, Tohoku Univ.) for their support of surface area measurement.

References

- Hoyer P (1996) *Langmuir* 12(6):1411
- Kasuga T, Hiramatsu M, Hoson A, Sekino T, Niihara K (1998) *Langmuir* 14(12):3160
- Gong D, Grimes CA, Varghese OK, Hu WC, Singh RS, Chen Z, Dickey EC (2001) *J Mater Res* 16(12):3331
- Oregan B, Gratzel M (1991) *Nature* 353(6346):737
- Adachi M, Murata Y, Takao J, Jiu JT, Sakamoto M, Wang FM (2004) *J Am Chem Soc* 126(45):14943
- Chou TP, Fryxell GE, Li XS, Cao G (2004) *Proc SPIE* 5510:129
- Jiu JT, Isoda S, Wang FM, Adachi M (2006) *J Phys Chem B* 110(5):2087
- Liu B, Aydil ES (2009) *J Am Chem Soc* 131(11):3985
- Kim EY, Choi H, Whang CM (2010) *J Mater Sci* 45(14):3895. doi:10.1007/s10853-010-4448-x
- Attar AS, Ghamsari MS, Hajiesmaeilbaigi F, Mirdamadi Sh, Katagiri K, Koumoto K (2008) *J Mater Sci* 43(17):5924. doi:10.1007/s10853-008-2872-y
- Mor GK, Varghese OK, Paulose M, Shankar K, Grimes CA (2006) *Sol Energy Mater Sol Cells* 90(14):2011
- Ghicov A, Albu SP, Hahn R, Kim D, Stergiopoulos T, Kunze J, Schiller CA, Falaras P, Schmuki P (2009) *Chem-Asian J* 4(4):520
- Asmatulu R, Karthikeyan A, Bell DC, Ramanathan S, Aziz MJ (2009) *J Mater Sci* 44:4613–4616. doi:10.1007/s10853-009-3703-5
- Kasuga T, Hiramatsu M, Hoson A, Sekino T, Niihara K (1999) *Adv Mater* 11(15):1307
- Shankar K, Mor GK, Prakasam HE, Yoriya S, Paulose M, Varghese OK, Grimes CA (2007) *Nanotechnology* 18(6):065707 (11 pp)
- Zhu K, Neale NR, Miedaner A, Frank AJ (2007) *Nano Lett* 7(1):69
- Uchida S, Chiba R, Tomiha M, Masaki N, Shirai M (2002) *Electrochemistry* 70(6):418
- Ohsaki Y, Masaki N, Kitamura T, Wada Y, Okamoto T, Sekino T, Niihara K, Yanagida S (2005) *Phys Chem Chem Phys* 7(24):4157
- Wei MD, Konishi Y, Zhou HS, Sugihara H, Arakawa H (2006) *J Electrochem Soc* 153(6):A1232
- Li XD, Zhang DW, Sun Z, Chen YW, Huang SM (2009) *Microelectron J* 40(1):108
- Chen Q, Zhou WD, Du DH, Peng LM (2002) *Adv Mater* 14(17):1208
- Tachikawa T, Tojo S, Fujitsuka M, Sekino T, Majima T (2006) *J Phys Chem B* 110(29):14055
- Ruan CM, Paulose M, Varghese OK, Mor GK, Grimes CA (2005) *J Phys Chem B* 109(33):15754
- Stergiopoulos T, Ghicov A, Likodimos V, Tsoukleris DS, Kunze J, Schmuki P, Falaras P (2008) *Nanotechnology* 19(23): 235602 (7 pp)
- Alivov Y, Fan ZY (2010) *J Mater Sci* 45(11):2902. doi:10.1007/s10853-010-4281-2
- Lei B-X, Liao J-Y, Zhang R, Wang J, Su C-Y, Kuang D-B (2010) *J Phys Chem C* 114(35):15228
- Zhu K, Neale NR, Halverson AF, Kim JY, Frank AJ (2010) *J Phys Chem C* 114(32):13433
- Lopez-Ayala S, Rincon ME, Pfeiffer H (2009) *J Mater Sci* 44(15):4162. doi:10.1007/s10853-009-3617-2
- Elsanousi A, Zhang J, Fadlalla HMH, Zhang F, Wang H, Ding X, Huang Z, Tang C (2008) *J Mater Sci* 43(11):7219. doi:10.1007/s10853-008-2947-9
- Ong KG, Varghese OK, Mor GK, Shankar K, Grimes CA (2007) *Sol Energy Mater Sol Cells* 91(4):250
- Kim J-Y, Sekino T, Park DJ, Tanaka S-I (2010) *J Nanopart Res*. doi:10.1007/s11051-010-9990-6
- Ovenstone J, Yanagisawa K (1999) *Chem Mater* 11(10):2770
- Djaoued Y, Bruning R, Bersani D, Lottici PP, Badilescu S (2004) *Mater Lett* 58(21):2618
- Kolen'ko YV, Garshev AV, Churagulov BR, Boujday S, Portes P, Colbeau-Justin C (2005) *J Photochem Photobiol A Chem* 172(1):19
- Cullity B (1978) *Elements of X-ray diffraction*. Addison-Wesley, Reading
- Van der Pauw LJ (1958) *Philips Research Reports* 13:1
- Chen SG, Chappel S, Diamant Y, Zaban A (2001) *Chem Mater* 13(12):4629
- Liu ZY, Pan K, Liu M, Wang MJ, Lu Q, Li JH, Bai YB, Li TJ (2005) *Electrochim Acta* 50(13):2583
- Schlichthorl G, Huang SY, Sprague J, Frank AJ (1997) *J Phys Chem B* 101(41):8141
- Zaban A, Greenshtein M, Bisquert J (2003) *ChemPhysChem* 4(8):859
- Ito S, Murakami TN, Comte P, Liska P, Gratzel C, Nazeeruddin MK, Gratzel M (2008) *Thin Solid Films* 516(14):4613
- Wang ZS, Kawauchi H, Kashima T, Arakawa H (2004) *Coord Chem Rev* 248(13–14):1381
- O'Regan BC, Durrant JR, Sommeling PM, Bakker NJ (2007) *J Phys Chem C* 111(37):14001